Supplementary Information for

Optical Kerr Nonlinearity and Ultrafast Photo-excited Carrier Dynamics in $CePO_4$/g-C_3N_4 Heterojunction: A Mechanistic Insight at 3D/2D Interface as Optical Power Limiter

Vijayakumar Balakrishnan[a], Venugopal Rao Soma[b] , Sabari Girisun Chidambaram[c], N Angeline Little Flower[a*]

[a] *Nanophotonics Research Laboratory, Department of Physics and Nanotechnology, SRM Institute of Science and Technology, Kattankulathur, Tamil Nadu, 603203, India*

[b]*School of Physics and DIA-CoE (formerly ACRHEM), University of Hyderabad, Hyderabad 500046, Telangana, India*

[c]*Nanophotonics Laboratory, Department of Physics, Bharathidasan University, Tiruchirappalli, 620024, India*

Corresponding author: N. Angeline Little Flower (angelin.flower@gmail.com)

Instrumentation

The phase purity and crystal structure analysis of the CP-gC powder sample were investigated using a PANalytical X' Pert PRO X-ray diffractometer at a wavelength of 1.5406 Å, which corresponds to Cu-Kα radiation. Thermal behaviour of the hybrid sample was examined using a SETARAM SETSYS Evolution 1750 instrument paired with thermogravimetric analysis and differential thermal analysis (DTA) measurements. An operational characterisation approach for visualising particles at the micro to nanoscale scale is Scanning Electron Microscopy (SEM). A Thermosceintific Apreo S SEM was used to analyse the sample morphology. It used Energy-dispersive X-ray Spectroscopy (EDS or EDX) as an analytical method to assess the sample chemical composition and analyse its constituent components. Using Shimadzu IR-Tracer infrared spectroscopy, the vibration modes of the synthesised CP-gC samples were investigated. By using X-ray photoelectron spectroscopy (XPS) technology, the relevant components chemical structure and oxidation state were verified. The synthesised CP-gC nanoparticles absorbance transition is shown by spectrophotometric UV-Vis analyses. A spectrofluorimeter was used to determine the photoluminescence emission spectra and the expected lifetime of the excited state electrons. Nanosecond and femtosecond laser pulses were used for nonlinear optical measurements. The Z-scan approach was used to assess the optical limiting threshold and nonlinear absorption under nanosecond pulses. The excitation source was a Nd: YAG nanosecond pulsed laser that operated at 532 nm with a pulse width of 9 ns.

Z-scan experiments were carried out with a repetition rate of 1 kHz using femtosecond pulses with an excitation wavelength of 800 nm and a pulse width of 35 fs. Studies on nonlinear refraction and absorption were carried out and nonlinear characteristics such absorption coefficient, second hyperpolarizability, refractive index, and third order susceptibility were determined.

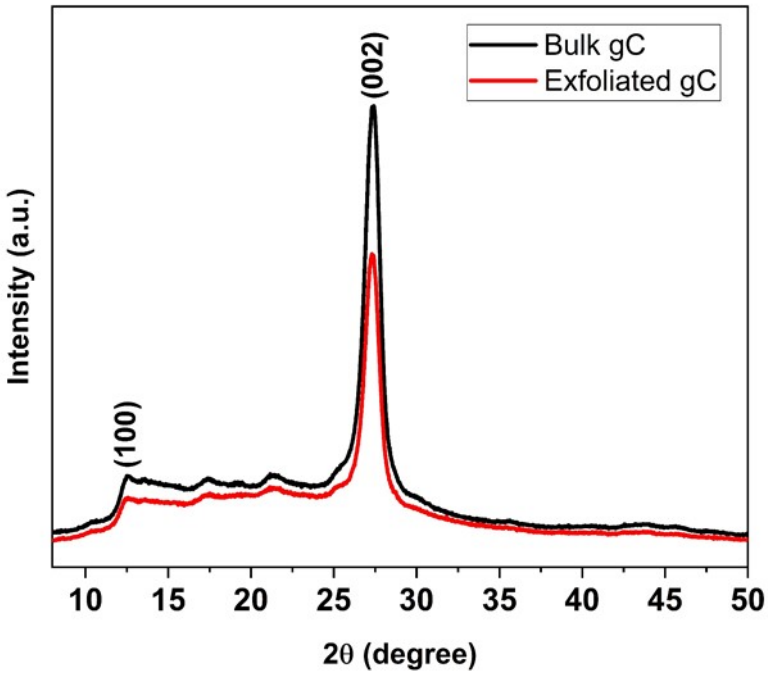

Figure S1. XRD plot of gC (bulk and exfoliated)

Williamson – Hall plot

Unlike the Scherrer equation, which shows a 1/cosθ dependency, the W-H approach shows a tanθ dependence. This fundamental difference helps to distinguish reflection broadening when small crystallite size and micro strain coexist as microstructural elements. According to the W-H approach, broadening of size and strain is a combined process influencing the total integral width of a Bragg peak. The effects of lattice distortion and crystallite size are evaluated independently using the W-H plot employing the uniform deformation model (UDM).[1]

$$\beta_{hkl} = \beta_S + \beta_D \quad \text{(S1)}$$

$$\beta_{hkl} = \frac{k\lambda}{DCos\theta} + 4\epsilon tan\theta \quad \text{(S2)}$$

β_{hkl}, β_S and β_D represents cumulative peak broadening, peak width due to lattice strain and grain size respectively.

Rearranging the equation S1 and S2, we get

$$\beta_{hkl} Cos\theta = \frac{k\lambda}{D} + 4\epsilon sin\theta \quad \text{(S3)}$$

The UDM model is represented by equation (S3), where strain is assumed to be uniform in all potential crystallographic orientations, recognising the crystal isotropic nature, where all material properties are independent of the direction of measurement. The Scherrer's crystallite size is denoted by D, the X-ray beam wavelength is λ (0.1541 nm for Cu-kα), the Bragg's diffraction angle is θ, the lattice strain is ε, and k is a constant (0.9 for spherical particles). Plotting the term (β cosθ) versus (4 sinθ) revealed the CP-gC samples preferred orientation peaks. Particle size and strain are represented by the y-intercept and slope of the fitted line, respectively.

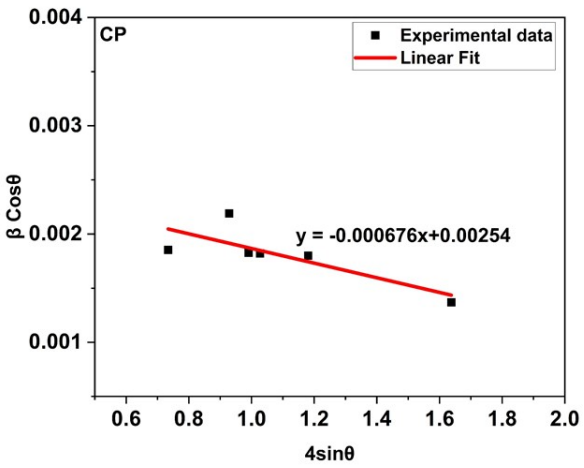

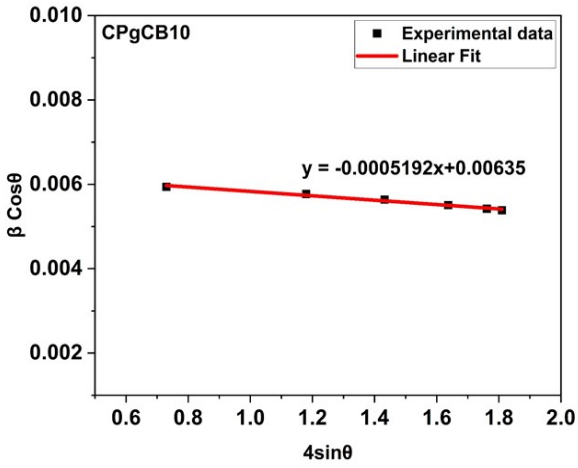

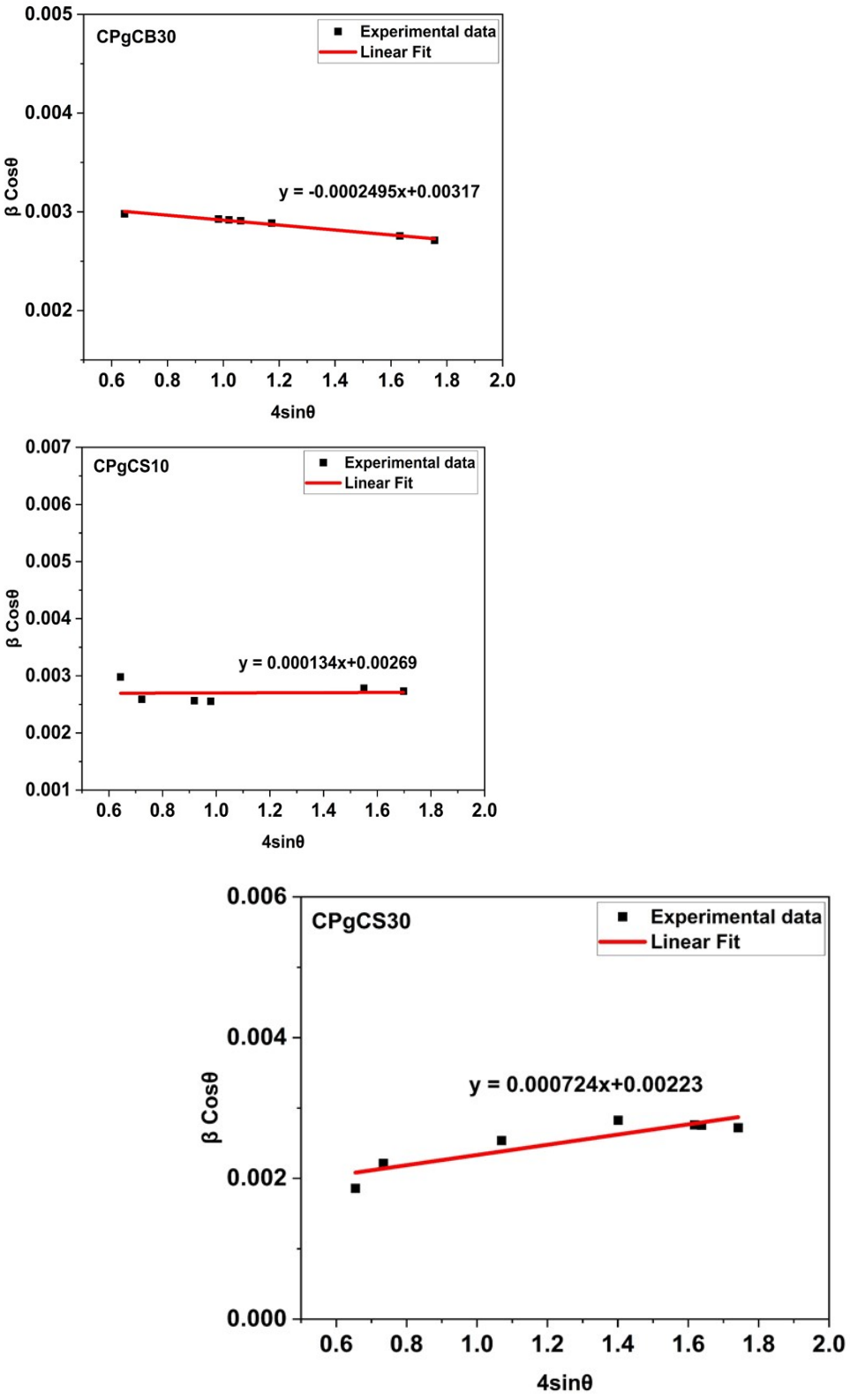

Figure S2. W-H plot for CP and CP-gC composites.

Table S1. Crystallite size and strain of CP-gC composites

Sample	Size from Scherer formula (nm)	Size from W-H plot (nm)	Strain
LP	46.2	51.1	-6.760×10^{-4}

LP-gCB10	18.5	20.6	-5.192×10^{-4}
LP-gCB30	41.3	41.0	-2.495×10^{-4}
LP-gCS10	45.6	48.0	1.348×10^{-4}
LP-gCS30	52.4	58.2	7.240×10^{-4}

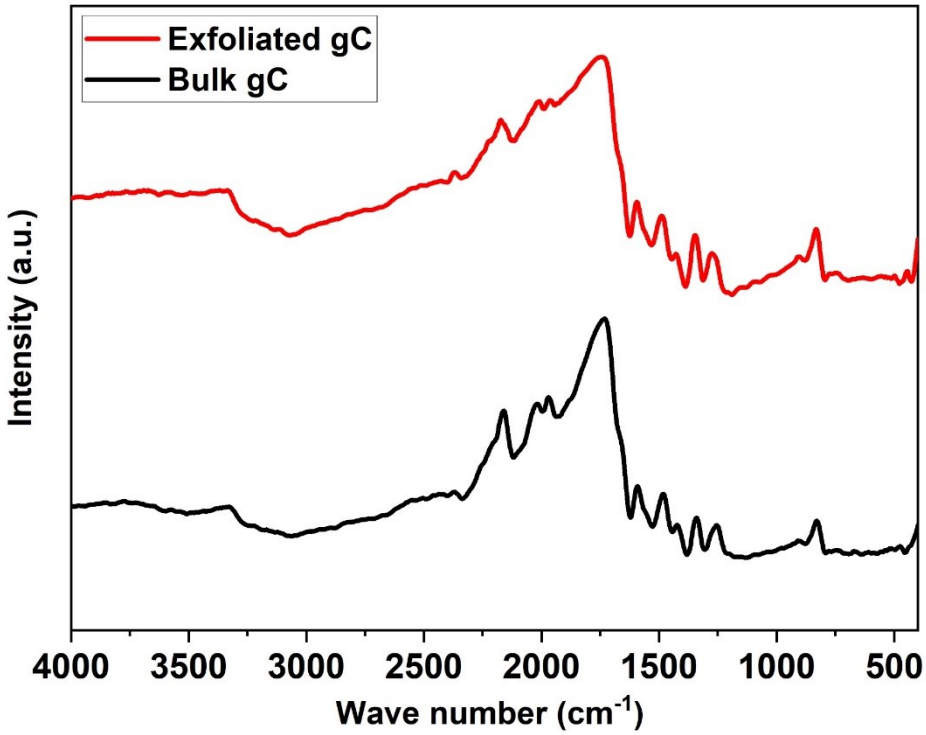

Figure S3. FTIR Spectra of gC

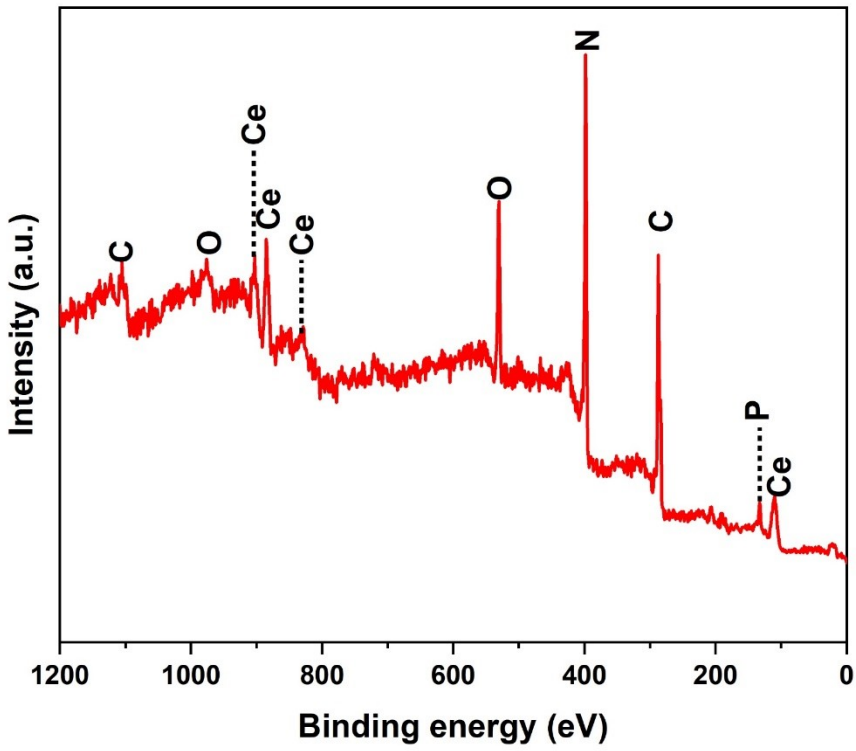

Figure S4. XPS survey spectra of CP-gCS30 composite.

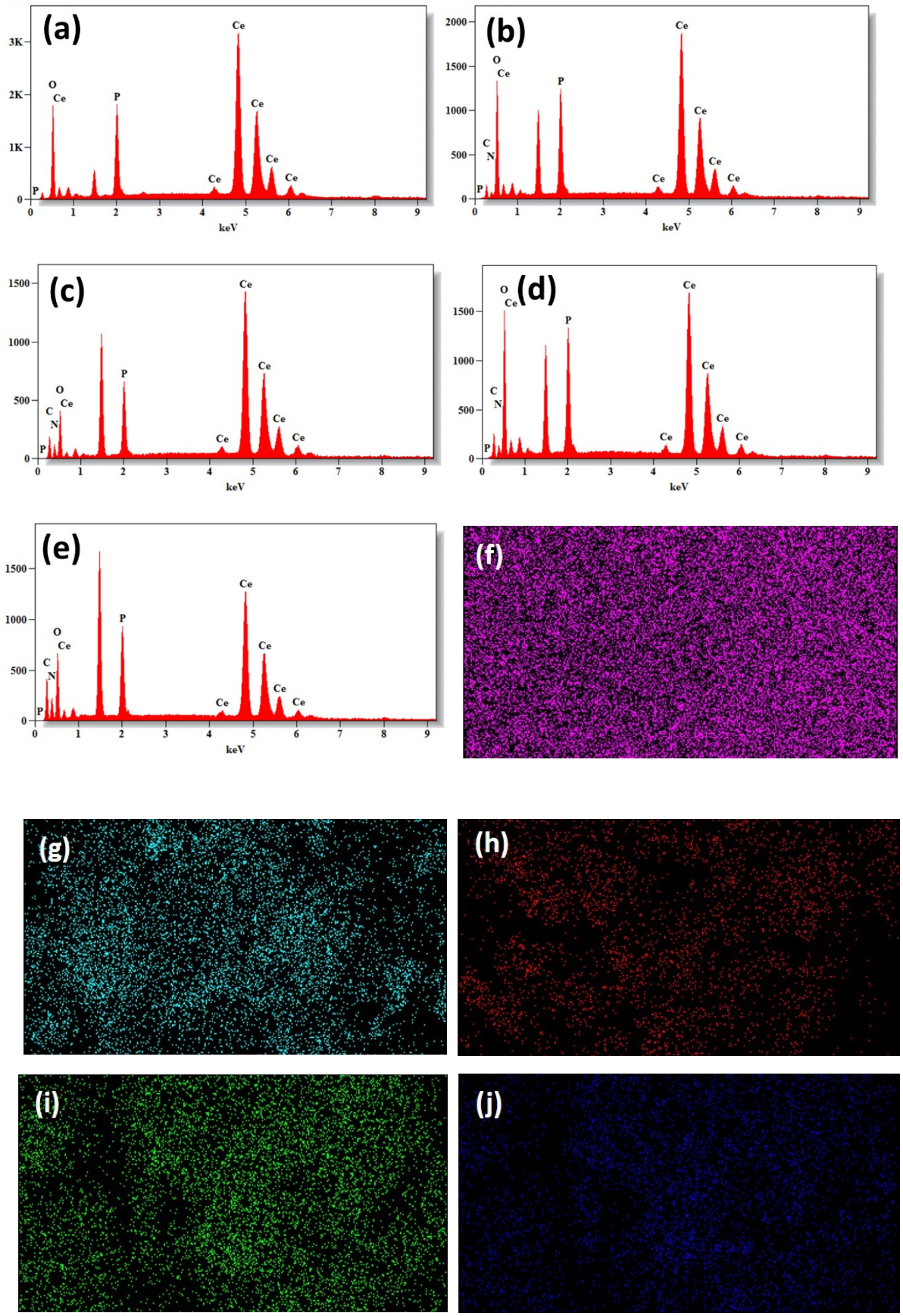

Figure S5. EDS spectra of (a) pure CP, (b-e) CP-gCB10, CP-gCB30, CP-gCS10 and CP-gCS respectively and EDS mapping of (f) Ce, (g) P, (h) O, (i) C and (j) N respectively of CP-gCS30 sample.

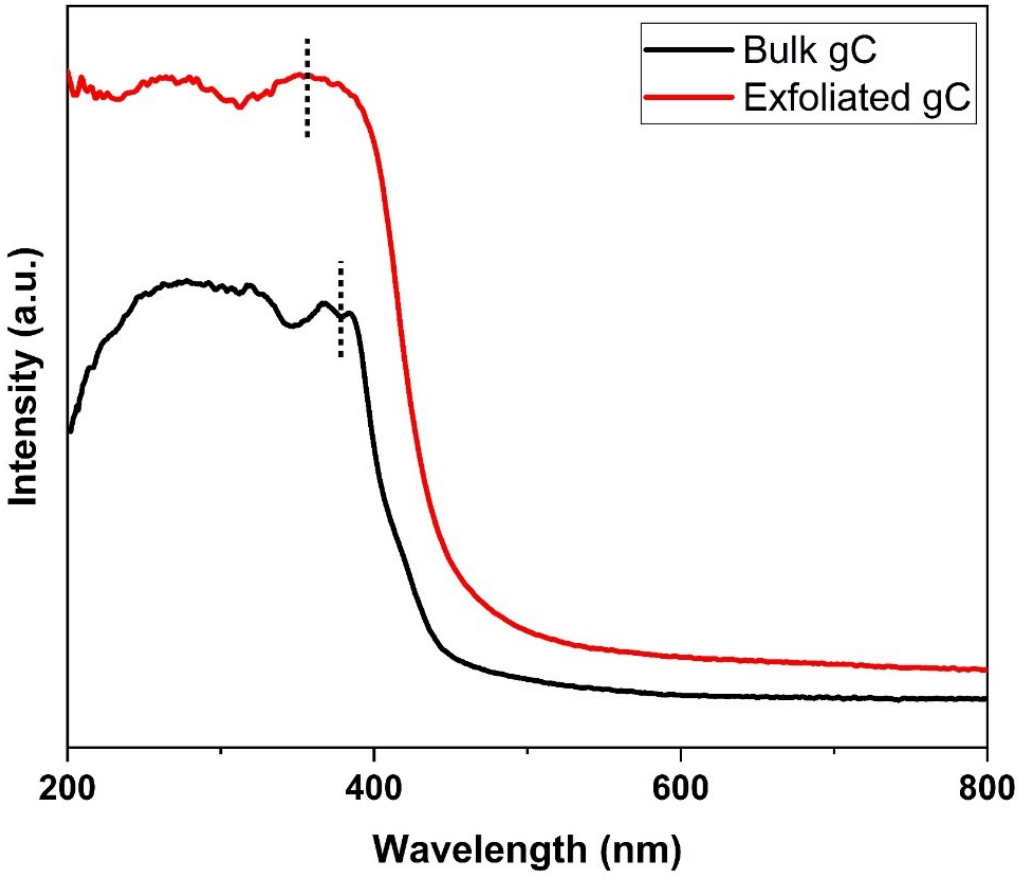

Figure S6. UV-Visible absorption spectra of bulk and exfoliated gC.

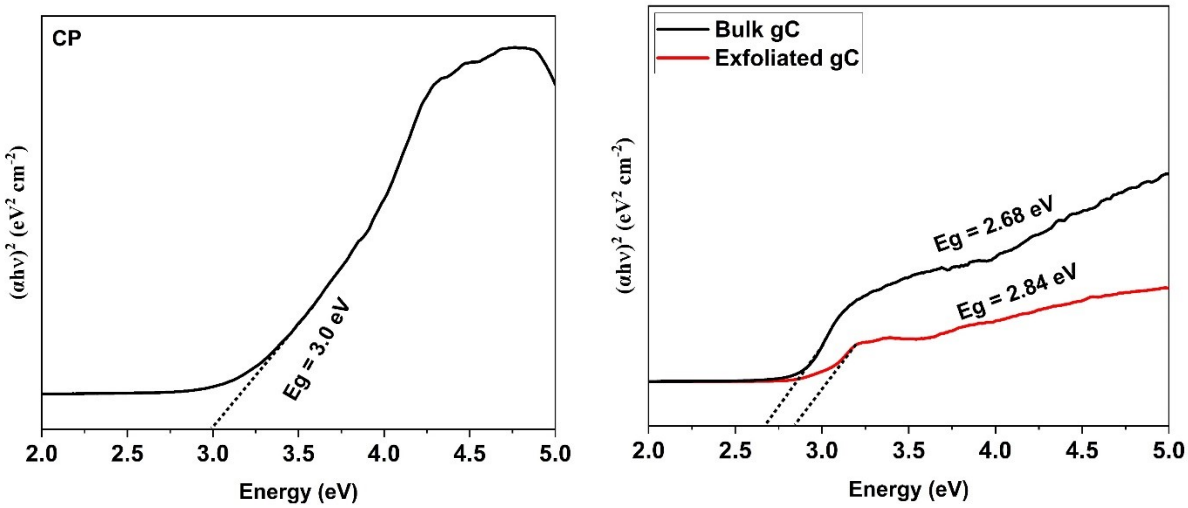

Figure S7. Band gap data of pure CP (left) and CP-gC composites (right)

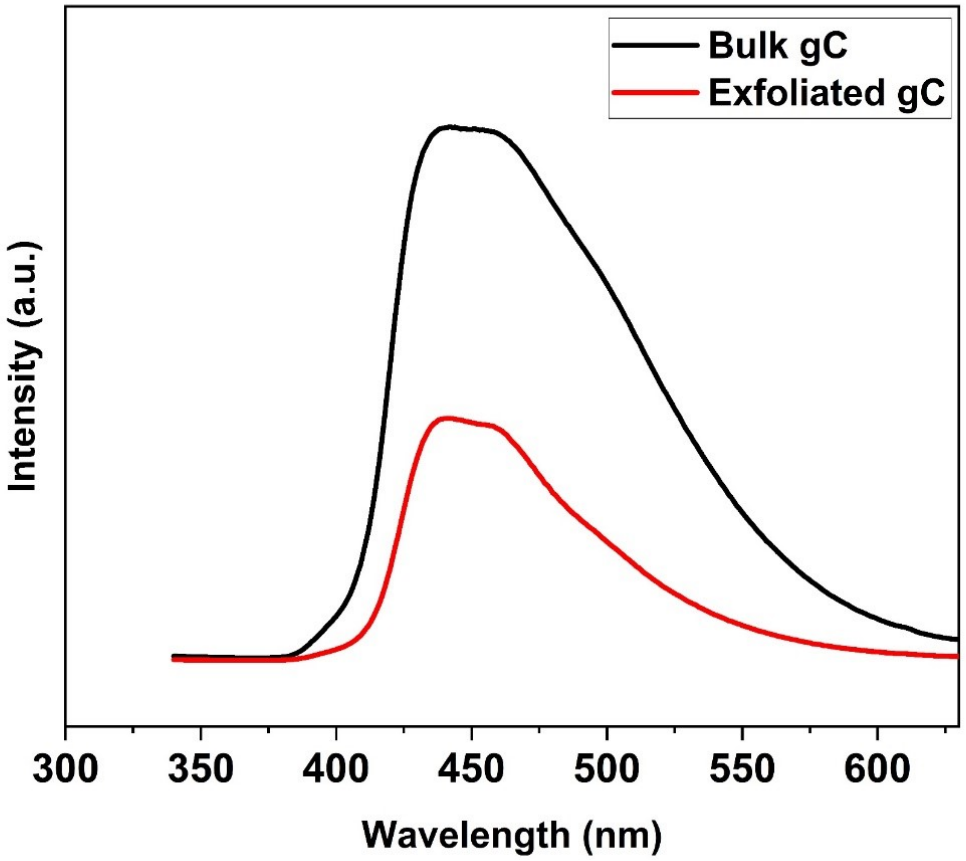

Figure S8. Emission spectra Bulk and exfoliated gC

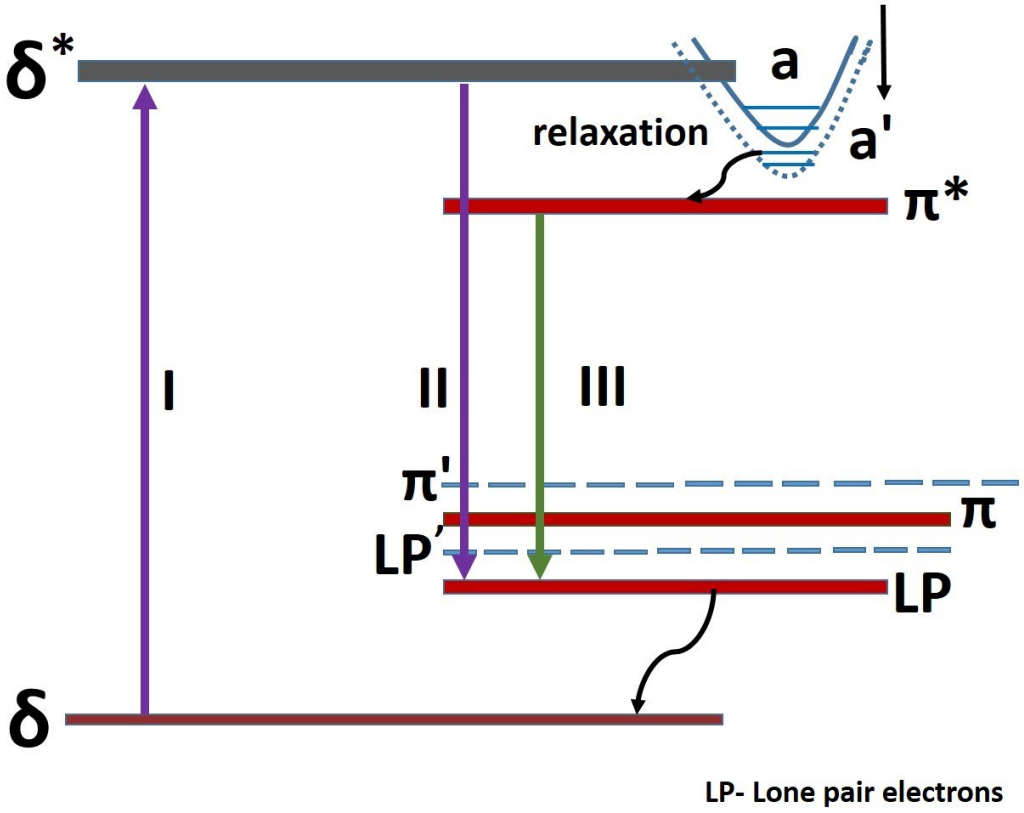

Figure S9. CP-gC composites energy level diagram

Table S2. Bi-exponential decay fit parameters of pure CP and LP-gC composites

Sample	I_1 (%)	τ_1 (ns)	I_2 (%)	τ_2 (ns)	τ_{avg} (ns)	χ^2
Pure CP	91.48	0.34	8.52	3.45	0.61	1.05
CP-gCB10	57.09	2.51	42.90	11.16	6.22	1.12
CP-gCB30	57.01	2.60	42.99	12.0	6.64	1.10
CP-gCS10	55.54	3.05	44.46	12.68	7.50	1.09
CP-gCS30	59.30	3.21	40.70	14.36	7.74	1.12

Table S3. CIE, colour purity of CP-gC composites

Sample	CIE (x,y)	Colour purity (%)
CP-gCB10	0.153,0.127	72.57
CP-gCB30	0.155,0.137	70.32
CP-gCS10	0.159,0.132	70.31
CP-gCS30	0.152,0.136	71.13

Computational details

Density functional theory calculations were performed with projected augmented wave (PAW) with Purdew, Berkey and Ernzerhof (PBE) psuedopotential, using Vienna *ab initio* simulation package (VASP). Ce valence electronic configuration 12 electrons: $5s^25p^66s^25d^14f^1$, P with $3s^23p^3$, and 6 in O $2s^22p^4$, 4 for C $2s^22p^2$ and 5 in N $2s^22p^3$. A cut off energy of 500 eV is applied for plane wave basis. In optimizing the geometry 10^{-6} eV/atom is used as convergence accuracy maximum convergence force between atoms was 0.01 eV. Cerium orthophosphate in P2*1/n* space group with monoclinic crystal structure exist with lattice parameters a= 6.43, b=7.02, c=6.52 Å confirmed by XRD analysis, is used for computational analysis. For gC in planar adjacent heptazine unit, a separation of 7.09-7.17 Å were considered to construct its super cell. Vaccum of 15Å was used over the super cell.

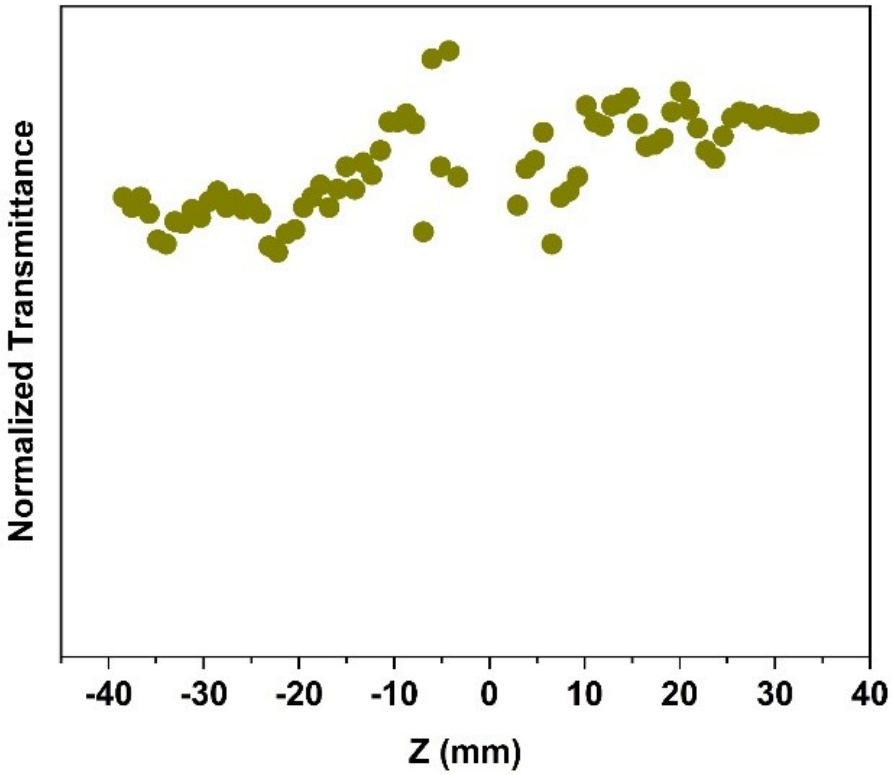

Figure S10. Femtosecond OA Z-scan pattern of DMF

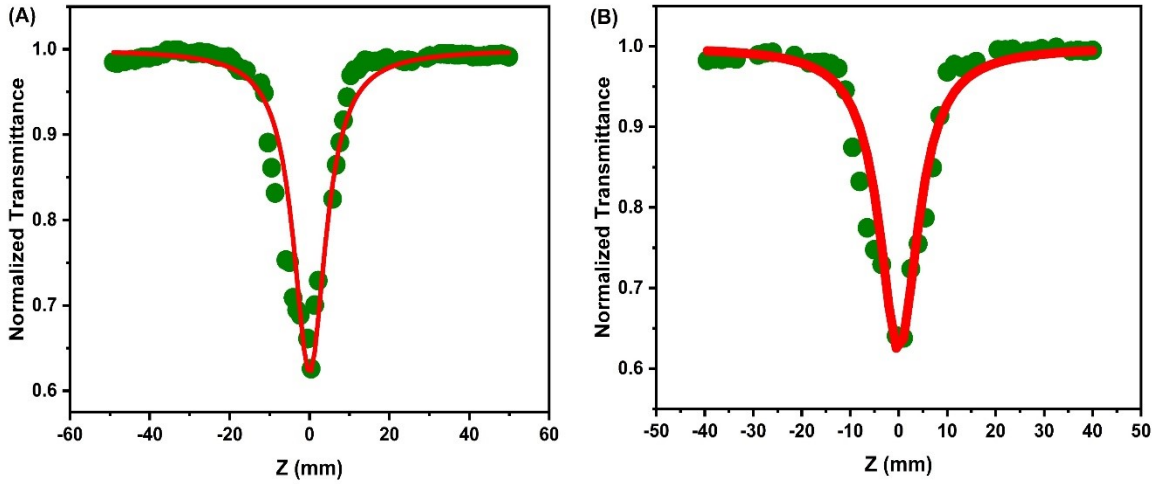

Figure S11. Femtosecond OA Z-scan curve (A) Bulk gC and (B) Exfoliated gC

Third order nonlinear susceptibility equation

$$Re\chi(3) = \frac{10^{-4}\epsilon_o c^2 n_o^2 n_2}{\pi} \quad \text{(S4)}$$

$$Im[\chi 3]\ (esu)\ = 10^{-2}\frac{\mathcal{E}_0\ n_0^2 c^2 \lambda}{4\pi^2}\ \beta\ \text{(cm/W)} \quad \text{(S5)}$$

In the above equation c denotes the speed of light, ϵ_o is permittivity of free space, n_2 represents the nonlinear refractive index and n_o linear refractive index.[2]

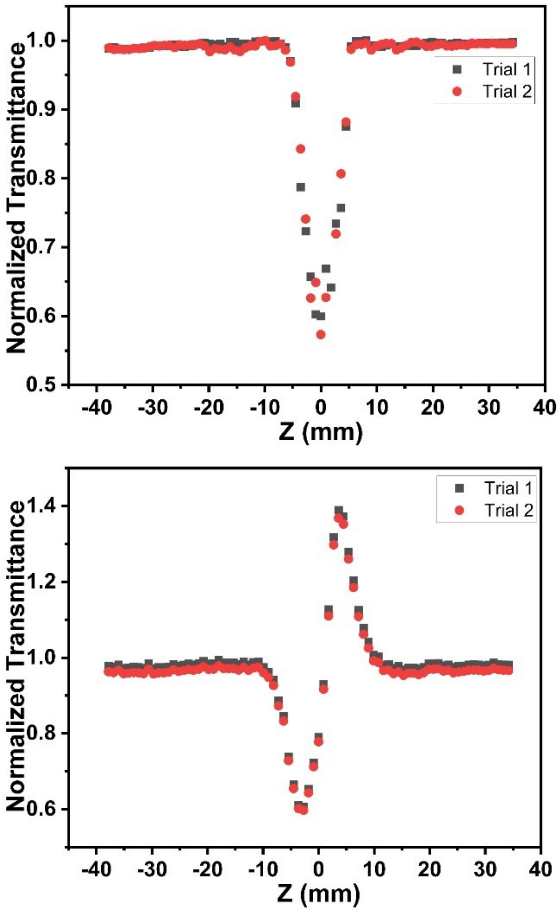

Figure S12. Photostability tests of CP-gCS30 sample at 100 nJ pulse energy.

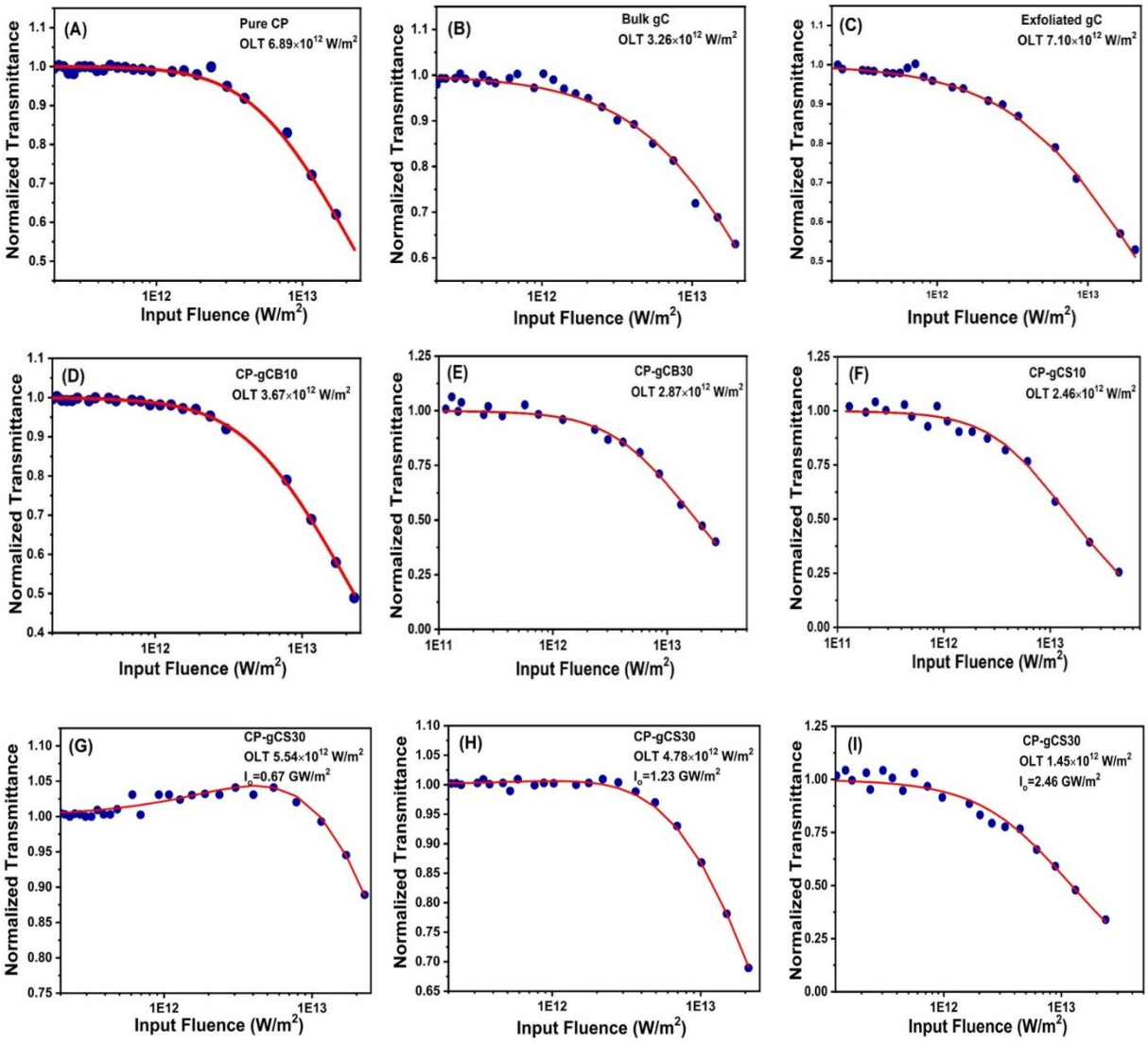

Figure S13. OL curves retrieved from nanosecond pulsed Z-scan data.

Relation between nonlinear refractive index and Kane energy

$$n_2 = \frac{K\hbar C\sqrt{E_P}}{n_0^2 E_g^4}\,\mathrm{G}\left(\frac{\hbar\omega}{E_g}\right) \quad \text{(S6)}$$

Here, E_g denotes energy band gap, $\mathrm{G}\left(\frac{\hbar\omega}{E_g}\right)$ is the dimensionless dispersion function, K is a material independent constant.

$$G(x) = \frac{-2 + 6x - 3x^2 - x^3 - \frac{3}{4}x^4 - \frac{3}{4}x^5 + 2(1-2x)^{\frac{3}{2}}\theta(1-2x)}{64x^6}$$

(x) denotes a Heaviside step function, such that $(x) = 0$ for $x < 0$ and $(x) = 1$ for $x \geq 0$.

$$K = \frac{2^9 \pi e^4}{5\sqrt{m_0} c^2}$$

m_o is the free electron mass.[3]

Kane energy is directly related to reduced exciton masss as

$$\mu = \frac{3 m_0 E_g}{2 E_p} \quad \text{(S7)}$$[4]

Table S4. Calculated value of E_P and μ

Sample	E_P (eV)	μ (with respect to electron rest mass m_o)
CP	24.9	0.26
CP-gCB10	23.2	0.24
CP-gCB30	23.4	0.23
CP-gCS10	23.0	0.25
CP-gCS30	23.1	0.27

References

[1] S. Dolabella, A. Borzì, A. Dommann, A. Neels, *Small Methods* **2022**, 6, 2100932.

[2] S. Bhattacharya, C. Biswas, S. S. K. Raavi, J. Venkata Suman Krishna, N. Vamsi Krishna, L. Giribabu, V. R. Soma, *The Journal of Physical Chemistry C* **2019**, 123, 11118.

[3] K. Ohara, T. Yamada, H. Tahara, T. Aharen, H. Hirori, H. Suzuura, Y. Kanemitsu, *Physical Review Materials* **2019**, 3, 111601.

[4] M. Sheik-Bahae, D. C. Hutchings, D. J. Hagan, E. W. Van Stryland, *IEEE Journal of quantum electronics* **1991**, 27, 1296.